coatings

MDPI

Article

Preparation of Chromium Carbide-Strengthened Ni-W Coatings by Electrodeposition and the Corresponding Anticorrosion Behavior in CO_2-Saturated NaCl Solution

Hongjie Li [1,*], Weizhi Zhang [2], Xi Yuan [1], Puzhi Li [3], Weilei Han [3] and Hongbing Huang [1]

[1] Research Institute of Natural Gas Technology, PetroChina Southwest Oil & Gasfield Company, Chengdu 610213, China
[2] PetroChina Oil, Gas & New Energies Company, Beijing 100007, China
[3] Southern Sichuan Gas District, PetroChina Southwest Oil & Gasfield Company, Luzhou 646000, China
* Correspondence: 18428301109@163.com

Abstract: In this study, we have prepared Ni-W/Cr_3C_2 composite electrodeposits through the diffuse reinforcement mechanism of chromium carbide nanoparticles. These electrodeposits exhibit excellent corrosion resistance and are designed to effectively protect the structural materials of pipe columns under the harsh CO_2 corrosion environments faced by carbon sequestration and utilization technologies. A systematic investigation was conducted into the micro-morphology, profile undulation, phase composition, and surface chemical state of the electrodeposits. Furthermore, the corrosion-resistant behavior of Ni-W/Cr_3C_2 composite electrodeposits was investigated in simulated corrosive environments (i.e., brine solution containing 3.5 wt% NaCl and CO_2-saturated brine). We then evaluated their corrosion response under the aforementioned conditions using electrochemical methods. In addition, the EIS of electrodeposited coatings revealed that the dense oxide film layer formed on the surface of the deposits, which acted as a primary barrier against corrosion, playing a pivotal role in maintaining the overall corrosion resistance of the material.

Keywords: Ni-W electrodeposits; chromium carbide; corrosion; carbon dioxide; brine

check for updates

Citation: Li, H.; Zhang, W.; Yuan, X.; Li, P.; Han, W.; Huang, H. Preparation of Chromium Carbide-Strengthened Ni-W Coatings by Electrodeposition and the Corresponding Anticorrosion Behavior in CO_2-Saturated NaCl Solution. *Coatings* **2024**, *14*, 1386. https://doi.org/10.3390/coatings14111386

Academic Editor: Kyong Yop Rhee

Received: 21 August 2024
Revised: 8 September 2024
Accepted: 10 September 2024
Published: 31 October 2024

Copyright: © 2024 by the authors. Licensee MDPI, Basel, Switzerland. This article is an open access article distributed under the terms and conditions of the Creative Commons Attribution (CC BY) license (https://creativecommons.org/licenses/by/4.0/).

1. Introduction

Against the backdrop of rapid global industrial development, the planet is facing an increasingly urgent challenge: climate warming [1,2]. This is mainly due to the large-scale emission of greenhouse gases, such as CO_2, into the atmosphere. In 2023, the United Nations Intergovernmental Panel on Climate Change (IPCC) released the AR6 Synthesis Report: Climate Change 2023 [3]. This report devotes nearly 8000 pages to detailing the devastating consequences of global warming caused by rising global greenhouse gas emission. Currently, all regions of the world are facing unprecedented changes in their climate systems because the global temperature has already risen by 1.1 °C. If global temperatures rise by more than 1.5 °C, regions depending on meltwater from snow and ice will face water scarcity so that they cannot adapt to this new environment. According to the above report, there is a more than 50% chance that the global temperature will rise to 1.5 °C or more between the years 2021 and 2040. To avoid this, global greenhouse gas emissions need to reach the peak value by the year 2025 at the latest, and then gas emissions will decline rapidly. Therefore, there is an urgent demand to control CO_2 emissions [4,5].

In this context, China has put forward a Chinese plan to address the challenge of carbon neutrality global governance to achieve carbon peaking and carbon neutrality. Carbon capture and storage (CCS), or carbon capture, utilization, and storage (CCUS), is considered to be one of the most effective ways to decrease CO_2 emissions [6–10]. CCS or CCUS is a process of injecting the captured CO_2 into the ground through engineering and technical means, and CCS or CCUS can also be used to produce and intensify the

extraction of energy and resources and then realize the long-term isolation of injected CO2 from the atmosphere. In China, large-scale CCUS projects have been carried out in Shengli Oilfield, Jilin Oilfield, Changqing Oilfield, and other fields [9,10]. In CCUS, steel corrosion occurs in multiple processes, such as CO_2 transportation, CO_2 flooding, and saline water storage [11]. Dried CO_2 is not corrosive, but in the process of CO_2 storage, transportation, and utilization, it will inevitably come into contact with water and other impurities [12]. Regarding carbonic acid, its acidity is often higher than that of hydrochloric acid at the same pH, resulting in the corrosion enhancement of steel [13]. Furthermore, in the CCUS process, a large amount of supercritical CO_2 is injected into the ground to enhance the efficiency of CO_2 sequestration, whereas a chemical reaction between CO_2 and the formation of water may occur to form highly corrosive carbonic acid, which, in turn, increases the risk of corrosion [14,15].

Currently, scientists and engineers have adopted a number of techniques to mitigate steel corrosion under CCUS conditions, such as CO_2 corrosion inhibitors, corrosion resistance alloy steel, and surface treatments [16–20]. Surface treatments can be a good method to control steel corrosion, and some previous works demonstrate the fact that electrodeposited Ni-W alloy coatings have a good potential to be applied to the CO_2 injection well [21,22]. Ni-W electrodeposits are a class of alloy coatings with industrial applications in the oil and gas industry. However, Ni-W electrodeposits are susceptible to defects, such as surface pinholes and microcracks, due to internal stress and hydrogen precipitation during the preparation process [23]. Researchers found that the composite electrodeposition technique can reduce the surface defects of the coatings by adding diffuse phase reinforcing materials [24–28]. Diffuse phase particles can reduce the internal stress of the coatings due to an increase in the deposit thickness by adsorbing more metal ions and refining the grains. It can also increase the structural strength of the deposit because of the diffuse phase strengthening effect.

Chromium carbide, a ceramic material, possesses wear, corrosion, and oxidation resistance [29–31]. Cr_3C_2-NiCr coatings are a class of widely used thermal spray coatings with Cr_3C_2 particles as the hard phase and Ni-Cr alloys as the binder phase in aircraft engines and petrochemical machinery devices [32–35]. Recently, Hosseinzadeh et al. prepared Ni/Cr_3C_2-NiCr composite coatings using the electrodeposition technique and found that the prepared coatings have excellent wear resistance [36]. Therefore, it can be believed that chromium carbide particles can be used as a diffuse phase material to strengthen the corrosion resistance of Ni-W coatings. However, there are no related studies currently.

In this study, Ni-W/Cr_3C_2 coatings were prepared by electrodeposit. Different characterization techniques were used to analyze the micro-profile, elemental distribution, and phase composition of the prepared coatings. Electrochemical impedance spectroscopy (EIS) was adopted to probe the corrosion resistance behavior of the prepared coatings in CO_2-saturated 3.5% NaCl brine under various test conditions.

2. Materials and Methods

2.1. Construct Ni-W/Cr_3C_2 Coatings

Typically, pulsed electrodeposition techniques were used to construct composite coatings, and the schematic diagram is shown in Figure 1. The parameters of electrodeposition could be seen in the authors' previous work [24]. The citrate–ammonium system was hired as the base bath solution, and the detailed parameters are shown in Table 1. The electrodeposition system utilized graphite plates (50 mm × 50 mm × 2 mm) as the anode and N80 steel sheets (30 mm × 15 mm × 3 mm) for the cathode, and the distance of the anode and cathode was 3 cm. Before electrodeposition, N80 steels were sanded and polished step by step before use. The chromium carbide ceramic particles were obtained from Zhejiang Yamei Nano Technology Co., Ltd., Jiaxing, China. All remaining chemicals were purchased from Chengdu Chron Chemicals Co., Ltd., Chengdu, China.

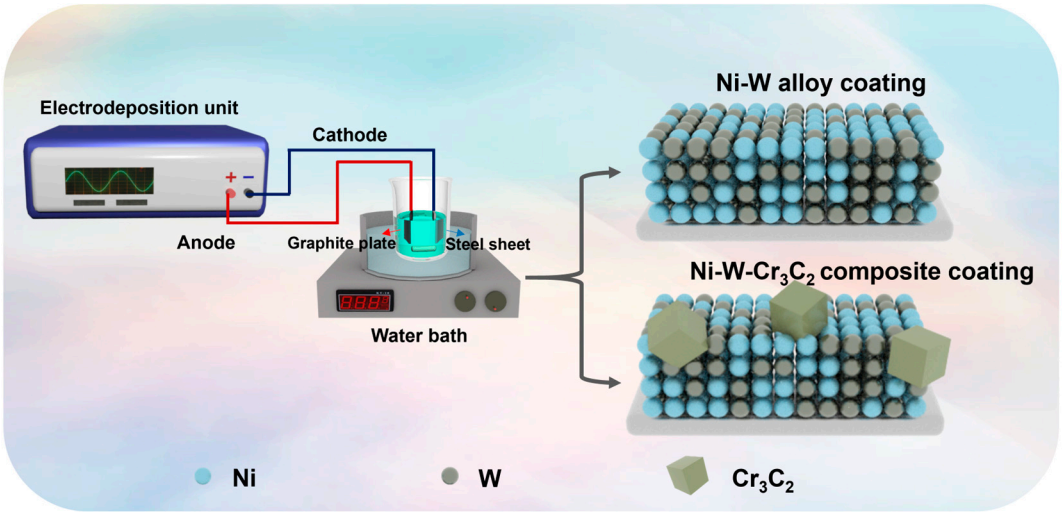


Figure 1. The schematic flow diagram of the constructed Ni-W/Cr_3C_2 electrodeposits.

Table 1. Process parameters and bath ingredients of Ni-W/Cr_3C_2 electrodeposits.

Ingredients	Content ($g \cdot L^{-1}$)	Plating Parameters	Value
Nickel sulfate	16	Current density	5 $A \cdot dm^{-2}$
Sodium tungstate	46	Pulse frequency	500 Hz
Sodium citrate	150	Duty cycle	80%
Sodium bromide	16	Time	45 min
Ammonium chloride	30	Temperature	70 ± 1 °C
SDS	0.1	pH	7.0 ± 0.1
Saccharin	1		
Chromium carbide	0.01/0.02/0.05/0.1		

2.2. Analysis and Characterizations of the Prepared Coatings

The contours of the prepared coatings and Cr_3C_2 powder were characterized by scanning electron microscopy (SEM, SEM, Phenom ProX Generation 5, Thermo Fisher Scientific, Breda, The Netherlands) and its accompanying 3D reconstruction system. The elemental distributions were analyzed using an energy-dispersive spectrometer (EDS). The chemical composition of the prepared coatings and Cr_3C_2 powder was explored by X-ray diffraction (XRD, X'Pert Pro MPD, Malvern Panalytical, Almelo, The Netherlands) and X-ray photoelectron spectroscopy (XPS, ESCALAB Xi +™ XPS Microprobe, Thermo Fisher Scientific, Breda, Netherlands). The size distributions and ζ-potential of Cr_3C_2 samples in brine were measured by Omni particle size and the zeta potential analyzer.

The corrosion resistance of the prepared coatings was evaluated by electrochemical impedance spectroscopy (EIS). EIS measurements were accomplished with a three-electrode system (CHI 760E), and the prepared coating specimens acted as the working electrode (WE) while a Pt plate operated as the counter electrode (CE). The saturated calomel electrode was the reference electrode (RE). The test vessel was a stainless-steel reactor with a three-electrode system that could be vented and exhausted, lined with corrosion-resistant polytetrafluoroethylene (PTFE), and the test medium was a 3.5% NaCl solution (Figure 2). The device could saturate the liquid phase with CO_2 and measure the corrosion resistance of the prepared coatings under atmospheric conditions. In this study, the test medium consisted of two cases: a 3.5% NaCl solution and CO_2-saturated 3.5% NaCl solution.

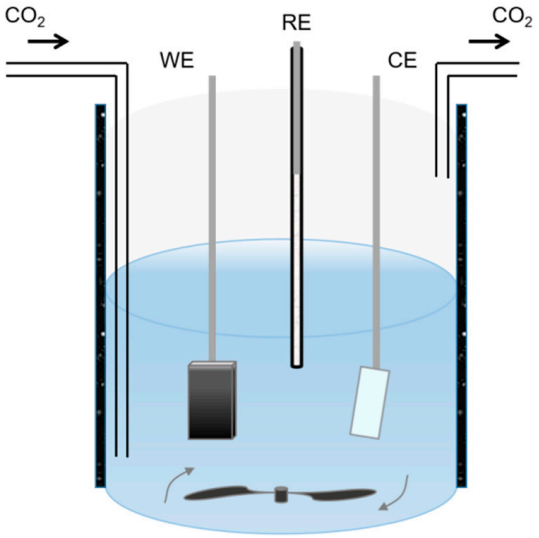


Figure 2. The schematic diagram of the electrochemical corrosion test device.

3. Results

3.1. Analysis of Chromium Carbide

The purchased Cr_3C_2 powders were observed by SEM (Figure 3A), and it could be seen that Cr_3C_2 powders have irregular profiles with dimensions in the order of a few micrometers. XRD is used to check the purity of bought chromium carbide (Figure 3B), and it can be observed that the characteristic peaks presented on its XRD pattern can be matched with the XRD standard card orientation of Cr_3C_2. As displayed in Figure 3B, the peaks situated in 32.6°, 35.2°, 39.0°, 40.2°, 42.6°, 45.5°, 46.6°, 47.5°, 48.0°, 48.6°, 50.1°, 51.2°, 54.1°, and 66.0° are be attributed to <1 1 1>, <1 0 4>, <1 1 2>, <2 0 3>, <1 0 5>, <2 0 4>, <2 1 1>, <0 0 6>, <1 1 4>, <2 1 2>, <3 0 1>, <0 1 5>, <1 1 5> and <0 2 0> crystalline planes of chromium carbide (PDF#71-2287) [30,31]. The XRD pattern also indicates that Cr_3C_2 belongs to the orthorhombic crystal system.

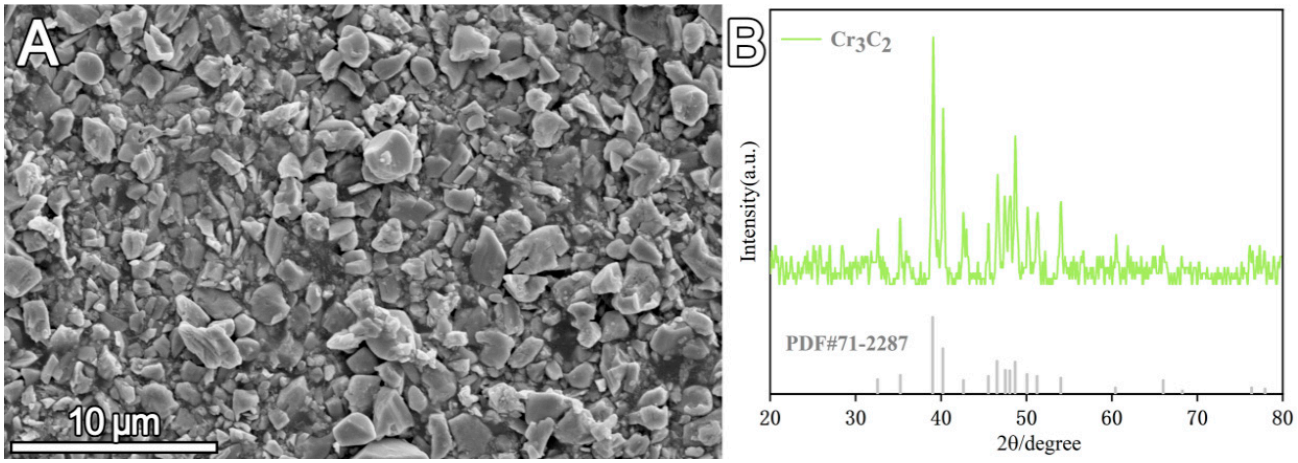


Figure 3. The SEM image (**A**) and XRD pattern (**B**) of purchased Cr_3C_2 powders.

Moreover, the dispersion and suspension behavior of chromium carbide particles in bath surroundings obtained by ζ-potential measurements and multi-angle light scattering tests are shown in Figure 4A. In systematic observations, the average size of Cr_3C_2 particles increases significantly with the increase in the concentration of particulate matter. At the same time, the ζ-potentials of these particles show a decreasing trend, which is a strong indication of agglomeration, i.e., the aggregation of smaller particles into larger

clusters due to the interaction effect. The agglomeration of particles, in turn, affects the overall particle size distributions and surface charge characteristics. Furthermore, as the scale of the cluster particles extends to the micrometer level, the ζ-potential value of the particulate matter decreases drastically to ~15 mV. Based on the classical theoretical framework of hydrophobic colloid stability, i.e., the DLVO (Derjaguin-Landau-Verwey-Overbeek) theory [37], this significant decrease in potential predicts a significant weakening of electrostatic repulsion between the particles. Meanwhile, the short-range forces, such as the van der Waals attraction, were relatively enhanced. Based on the classical framework of the DLVO theory, this significant decrease in potential signifies a weakening of the electrostatic repulsion between particles, while short-range forces, such as van der Waals attractions, were relatively strengthened. Under these conditions, the stability of the whole suspension system was destroyed, and the original dynamic equilibrium was no longer maintained, but it tended to undergo significant sedimentation phenomena, which marked the transition from the dispersed state to the aggregated sedimentation state.

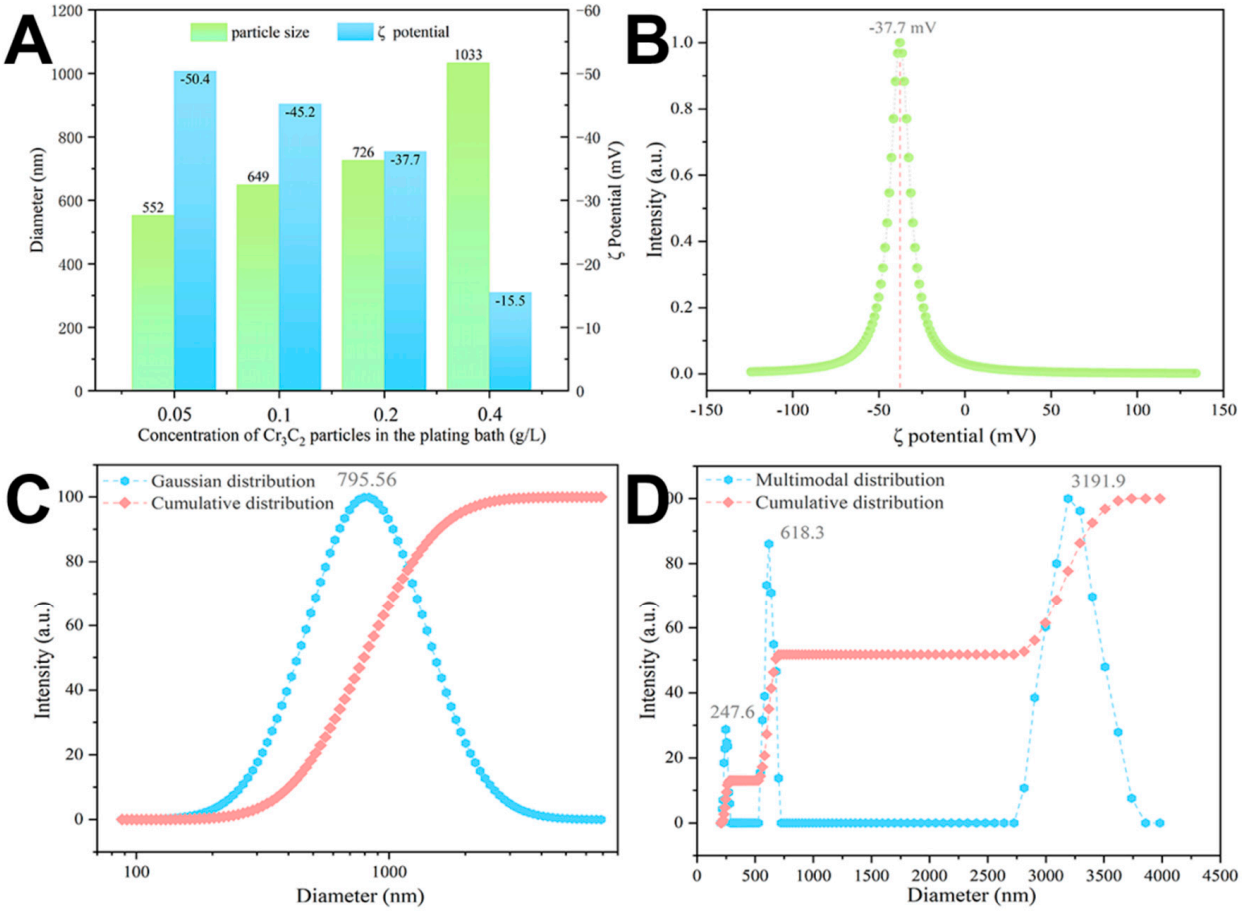


Figure 4. (**A**) Comparison of particle size distribution and ζ-potential data for different concentrations of Cr_3C_2 particles in the bath; (**B**) the ζ-potential curve; (**C**) the Gaussian size distribution; and (**D**) the multimodal size distribution of Cr_3C_2 particles in the bath with a concentration of 0.2 g/L.

Therefore, based on the variation in the concentration gradient of the experimental setup and the test results, it is more typical to select the bath at a chromium carbide concentration of 0.2 g/L for detailed characterization. The ζ-potential curves show that the suspended solids system can still be stabilized under this condition, as seen in Figure 4B. Figure 4C illustrates the Gaussian distribution profile of the suspended matter dispersion, while Figure 4D reflects its multi-peaked distribution profile. The Gaussian distribution curve states that the mean size of Cr_3C_2 particles in this circumstance was around 800 nm. The multimodal distribution curves reveal that Cr_3C_2 particles may have three agglomer-

ated forms in bath with sizes of about 250 nm, 600 nm, and 3 µm, which may be single particles, two-particle stacks, and multi-particle agglomerates, respectively.

3.2. Characterizations of the Prepared Coatings

The micro-morphology of the different Ni-W-Cr_3C_2 coatings is exhaustively observed using SEM, as shown in Figure 5. The results demonstrate that the surface of the pure alloy electrodeposits exhibits smoothness and homogeneity. However, with the gradual increase in the content of dispersed phase particles embedded in the coatings, a significant increase in the grain size of the deposit surface is observed. This phenomenon can be attributed to the fact that the particles in solution act as nucleation centers during the deposition process, attracting and promoting the aggregation of surrounding metal ions and accelerating the deposition of the particles on the substrate material [24], which, in turn, promotes the coarsening of the grains. This attraction is mainly due to the ζ-potential and double electric layer on the surface of the particle, and upon adsorption of the surrounding ions, the charged nature of the particle changes, which, in turn, promotes the deposition effect of the complexes. The parts circled in red in the images can be observed as hard particles embedded in the coating. Furthermore, it is demonstrated that the defect density on the deposited surface increases in direct proportion to the increase in the embedded number of particles in the diffuse phase. This is primarily attributed to the desorption of particulate matter during the electrodeposition process, which results in the formation of voids or uneven areas on the surface of the plated layer, leading to the formation and growth of defects. Furthermore, Figure 5F,G illustrate the mosaic of diffuse phase particles present in the sediment.

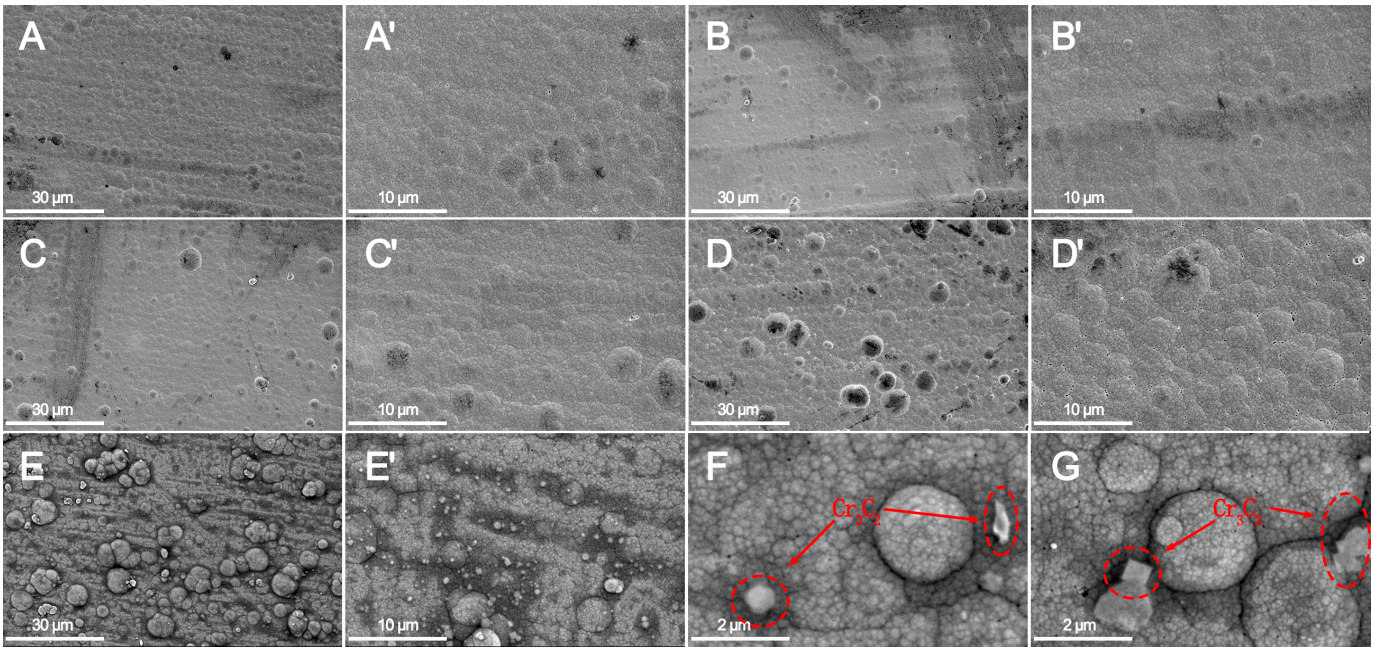


Figure 5. The SEM images of Ni-W-Cr_3C_2 electrodeposits with different concentrations of Cr_3C_2 particles in the bath under two magnification levels: (**A**,**A′**) 0 g/L, (**B**,**B′**) 0.05 g/L, (**C**,**C′**) 0.1 g/L, (**D**,**D′**) 0.2 g/L, and (**E**,**E′**) 0.4 g/L. The image (**F**,**G**) illustrates the presence of Cr_3C_2 particles within the electrodeposits.

The 3D reconstruction software, which is included with SEM, is employed with the objective of achieving a detailed observation and analysis of the surface micro-morphology of the prepared coatings, as exhibited in Figure 6. As can be observed in Figure 6, the different colors represent the microscopic undulations of the sediment surface. Regarding the color is blue, it is the deepest depression or the flattest ground. If the color is red, it

is the highest surface undulation. However, if the color is green or yellow, it has average roughness. It can be observed that the surface roughness of the prepared coatings is significantly enhanced as the amount of chromium carbide increases. This supports the hypothesis that Cr_3C_2 can accelerate the deposition of metals. However, the over-quick deposition also causes an increase in the number of defects on the surface of electrodeposits.

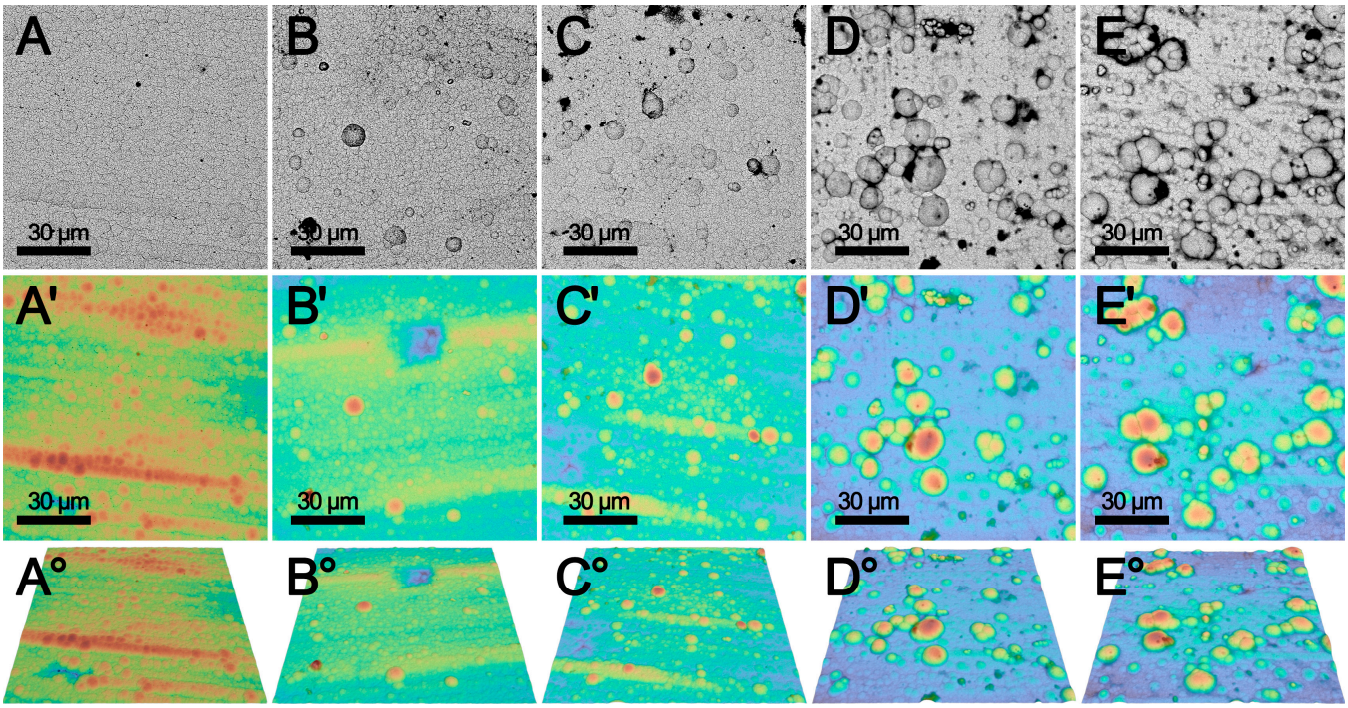


Figure 6. The 3D contour reconstruction image based on the SEM of Ni-W-Cr_3C_2 electrodeposits with different concentrations of Cr_3C_2 particles in the bath: (**A**) 0 g/L, (**B**) 0.05 g/L, (**C**) 0.1 g/L, (**D**) 0.2 g/L, and (**E**) 0.4 g/L. Letters indicate SEM images of the scanned area, while the superscripts ′ and ° are used for 2D and 3D reconstructed images.

In this study, Ni-W-Cr_3C_2 coatings prepared at a chromium carbide particle concentration of 0.2 g/L in the plating solution were selected as samples for EDS characterization. In the EDS mapping (Figure 7), the Cr_3C_2 particles are clearly identified to be uniformly embedded in the surface layer of the deposit, demonstrating good dispersion of chromium carbide and no significant particle agglomeration. Furthermore, EDS spectroscopy (Figure 8) demonstrates that the prepared coatings are predominantly composed of approximately 80 wt% nickel, 20 wt% tungsten, and trace amounts (approximately 1 wt%) of Cr_3C_2.

Furthermore, a systematic evaluation of the specific effect of chromium carbide on the deposition rate is conducted through an elemental composition analysis of the sample cross-section, as shown in Figure 9. The experimental results demonstrate that the thickness of the Cr_3C_2-doped composite coatings (~24 μm) is significantly greater than that of the pure alloy deposits (~19 μm). This finding indicates that the introduction of Cr_3C_2 can increase the deposition rate by approximately 30% in an equivalent electrodeposition cycle. This observation strongly demonstrates that chromium carbide can effectively enhance the efficiency and deposition rate through its unique surface adsorption property, which enables it to capture surrounding metal ions through the mechanism of the local discharge effect.

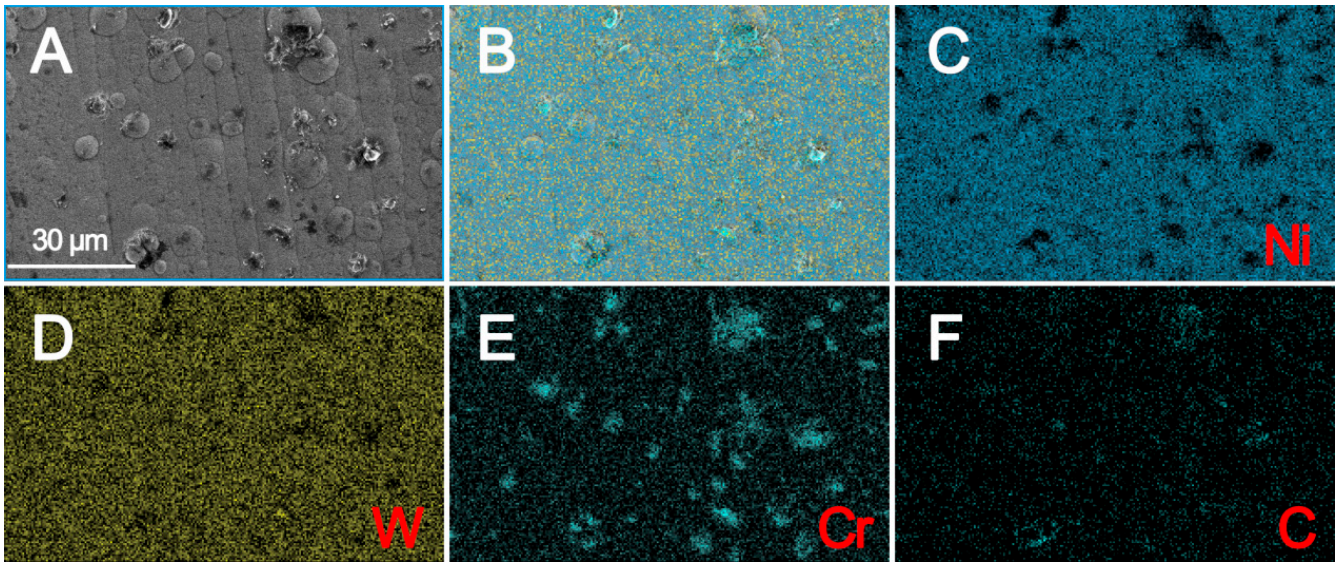


Figure 7. The EDS mapping images of Ni-W-Cr_3C_2 electrodeposits: (**A**) the selected SEM, (**B**) overlap mapping, (**C**) Ni mapping, (**D**) W mapping, (**E**) Cr mapping, and (**F**) C mapping.

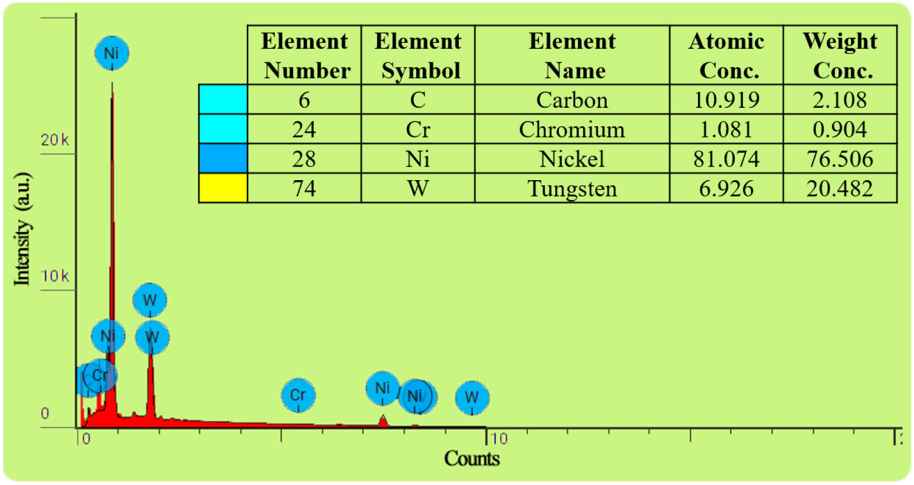


Figure 8. The EDS spectrum of Ni-W-Cr_3C_2 electrodeposits.

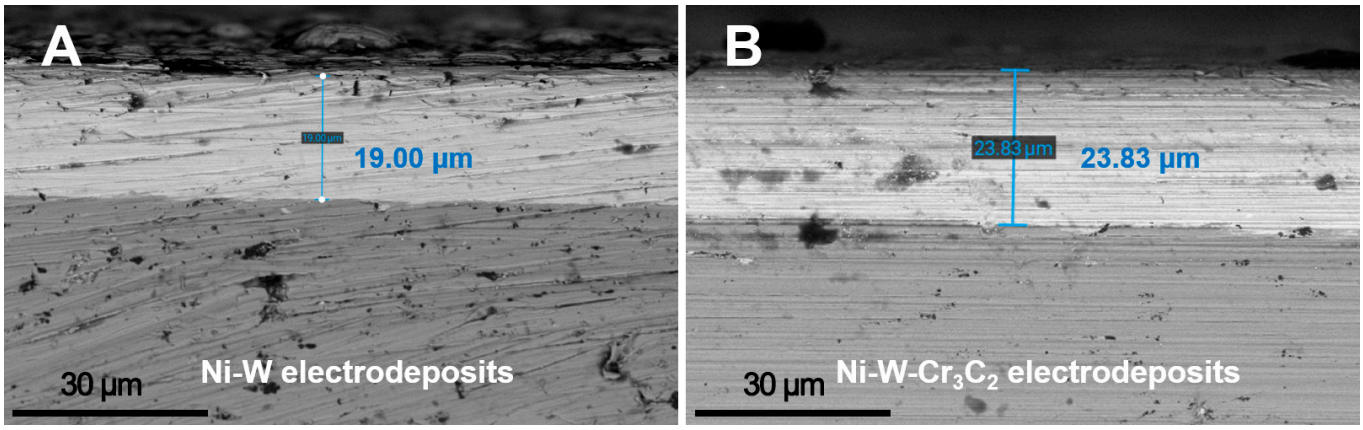


Figure 9. The SEM image of a cross-section of alloy electrodeposits (**A**) and the Ni-W-Cr_3C_2 electrodeposits (**B**).

The chemical composition of the prepared coatings and their crystalline properties were systematically investigated using the XRD technique, as shown in Figure 10. A series of diffraction peaks typical of nickel-based alloys can be identified in the resulting XRD patterns, with peak positions of 44.6°, 51.9°, and 76.4° clearly corresponding to the <1 1 1>, <2 0 0>, and <2 2 0> crystalline reflections of the face-centered cubic (FCC) nickel structure [24–26]. While tungsten is incorporated into the nickel matrix as a solid solution-strengthened phase, the FCC alloys have a number of advantages due to their unique crystal structure, including excellent plasticity, outstanding low-temperature performance, high densities, and corrosion resistance. It is worth noting that tungsten can also form crystalline phases under electrodeposition conditions, as evidenced by XRD patterns at 44.8° and 78.2°, attributed to the <2 0 0> and <3 1 1> crystallographic planes of body-centered cubic (BCC) tungsten [27,28], respectively. It is shown that W element doping not only involves a variety of strengthening mechanisms, such as solid solution strengthening, fine grain strengthening, and second phase strengthening (involving the μ-phase, σ-phase, and b.c.c. phase, etc.) [38] but also promotes the formation of a dense WO_3 passivation film on the surface of the alloy, which significantly improves the corrosion resistance of the material [39]. In addition, as the Cr_3C_2 concentration increases, characteristic diffraction peaks corresponding to chromium carbide can also be observed in the XRD patterns. This finding provides an important basis for the further understanding of the microstructure of the composite electrodeposits and their performance correlation.

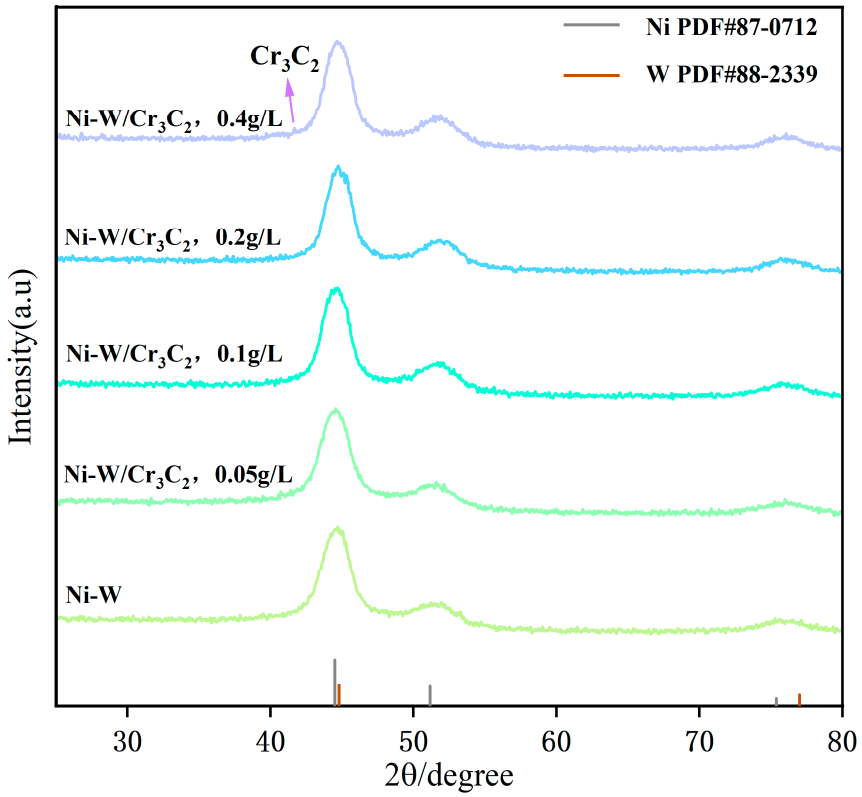


Figure 10. The XRD pattern image of Ni-W-Cr_3C_2 electrodeposits with different concentrations in the bath.

Furthermore, the chemical state of the elements on the surface of the prepared coatings is investigated in depth using the XPS technique (Figure 11). The characteristic peaks of C 1s, Ni 2p, W 4f, and Cr 2p are clearly identified in the global scanning spectra, and these peak positions provide a foundation for subsequent element-specific analysis. Subsequently, detailed analysis is carried out for the spectra of each element. The Ni 2p spectrum exhibits the characteristic peaks of metallic nickel, as well as oxidized nickel

(mainly NiO or $Ni(OH)_2$) [27]. This indicates the formation of a dense nickel oxide film on the surface of the electrodeposits, which is well known for its excellent anticorrosive properties. Similarly, the W 4f spectral analysis revealed the coexistence of metallic tungsten and tungsten oxide species, and the formation of WO_X film layers, likewise, have a positive effect on enhancing the corrosion resistance of the Ni-W-Cr_3C_2 coatings [27,28].

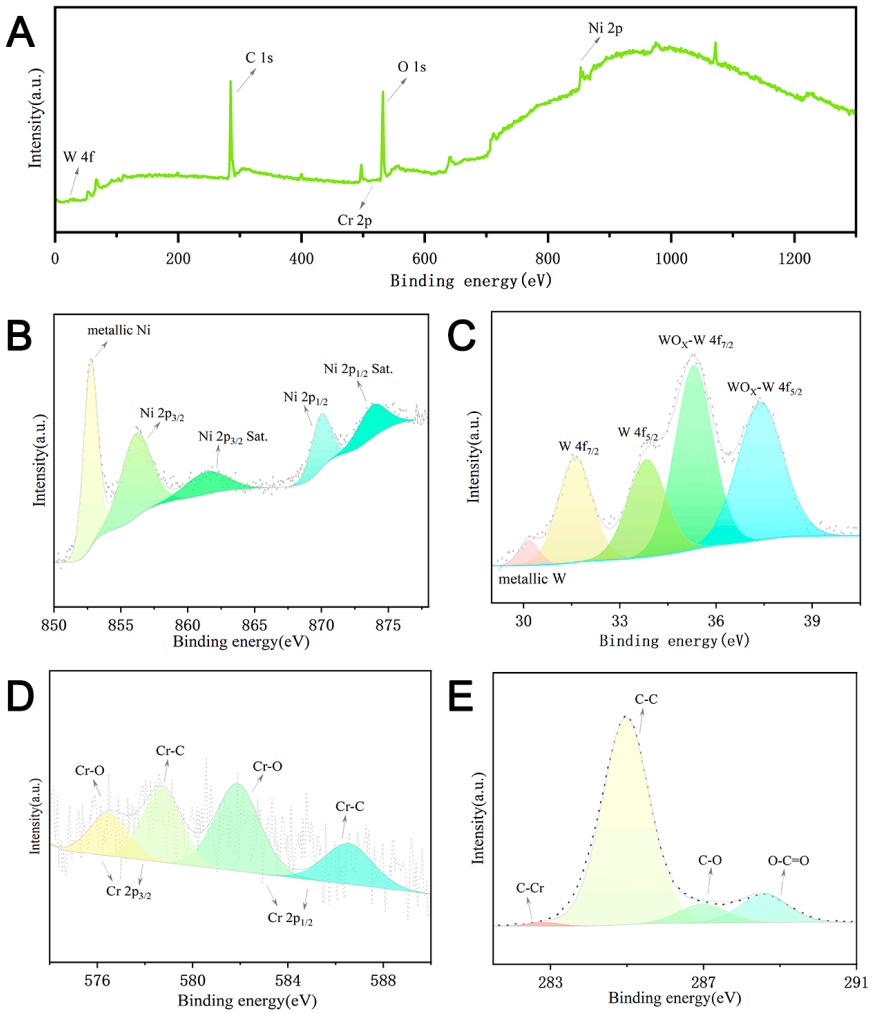


Figure 11. The XPS spectrum of Ni-W-Cr_3C_2 electrodeposits. (**A**) the full XPS spectrum of Ni-W-Cr_3C_2 electrodeposits. (**B**) the high-resolution spectrum of Ni. (**C**) the high-resolution spectrum of W. (**D**) the high-resolution spectrum of Cr. (**E**) the high-resolution spectrum of C.

Moreover, the presence of Cr 2p characteristic peaks directly demonstrates the successful incorporation of chromium carbide on the surface of the prepared coatings. Its spectral characteristics indicate that the Cr element is predominantly present in the form of a Cr-C bond in chromium carbide, while the surface is also coated with a layer of chromium oxide consisting of a C-O bond [34,35]. The latter is recognized as an excellent corrosion-resistant material, which further enhances the overall corrosion resistance. In conclusion, XPS spectroscopic analysis not only reveals the complex multi-element chemical states on the surface of the prepared coatings but also elucidates the manner in which these elements interact to construct a multi-layered, dense oxide film layer on the surface with excellent corrosion resistance. This finding indicates the application potential of Ni-W-Cr_3C_2 electrodeposits in highly corrosive environments.

3.3. Electrochemical Behaviour of the Prepared Coatings

The implementation of CCUS technology presents a significant challenge in the form of corrosion risks for downhole tubulars, which are essential components of this technology. These risks are present throughout both the injection and extraction processes, which require the tubular column to withstand the complex formation environment and the corrosive nature of the highly mineralized formation of water. Additionally, the column must resist the continuous erosion of metal surfaces by CO_2 and its associated gases [11,12]. The formation of water and other water-bearing fluids mix with CO_2, forming carbonic acid and causing the total and localized pitting corrosion of the pipe [14]. In addition, highly mineralized formation water and chloride ions in the drilling fluid promote the occurrence of pitting corrosion of the pipe columns [21,22].

Typically, the corrosion process of carbon steel is demonstrated below:

$$Fe \rightarrow Fe^{2+} + 2e^{-} \quad (1)$$

$$O_2 + 2H_2O + 4e^{-} \rightarrow 4OH^{-} \quad (2)$$

$$Fe^{2+} + 2OH^{-} \rightarrow Fe(OH)_2 \quad (3)$$

$$Fe(OH)_2 + e^{-} + OH^{-} \rightarrow Fe(OH)_3 \quad (4)$$

$$2Fe(OH)_3 \rightarrow Fe_2O_3 + 3H_2O \quad (5)$$

$$Fe(OH)_2 + 2Fe(OH)_3 \rightarrow Fe_3O_4 + H_2O \quad (6)$$

In order to evaluate the corrosion resistance of Ni-W-Cr_3C_2 electrodeposits, we employed EIS to ascertain their electrochemical anti-corrosion behavior, as shown in Figure 12 and Table 2. The analog circuit model is R(Q(R(QR))), and EIS data were fitted with ZSimpWin 3.30 software. The solution resistance (R_s), film resistance (R_f), and charge transfer resistance (R_{ct}) were the three parameters. CPE, i.e., the constant phase element, is a term commonly used to describe the behavior of a non-ideal electrical double-layer capacitor. The non-ideal, purely capacitive behavior of CPE elements is typically attributed to electrode surface inhomogeneities, roughness, the porosity of the electrodes, and non-uniformity of current and potential distributions associated with the electrode geometry. It is generally accepted that the corrosion resistance of electrodeposited coatings can be quantified and evaluated by the impedance value in the EIS. This is expressed as the sum of R_s, R_f, and R_{ct}. This comprehensive impedance index, which is a key parameter for evaluating the corrosion resistance of coatings, can effectively reflect the stability and protection effectiveness of coatings in corrosive environments.

Table 2. The equivalent circuit model parameters of the EIS test in the brine contain 3.5% NaCl of the Ni-W-Cr_3C_2 coatings.

Cr_3C_2 Amount	R_s (Ω)	CPE_f ($\Omega^{-1}\cdot cm^{-2}\cdot s^n$)	R_f (Ω)	CPE_{ct} ($\Omega^{-1}\cdot cm^{-2}\cdot s^n$)	R_{ct} (Ω)	R (Ω)
0	1.613	1.439×10^{-4}	920.9	1.196×10^{-5}	4166	5089
0.05	3.653	2.752×10^{-5}	1527	0.983×10^{-4}	4349	5880
0.1	1.162	9.389×10^{-5}	6438	1.035×10^{-5}	2437	8876
0.2	1.968	3.617×10^{-5}	9413	1.444×10^{-4}	7906	17,321
0.4	2.556	7.701×10^{-6}	223.2	3.421×10^{-4}	2085	2311

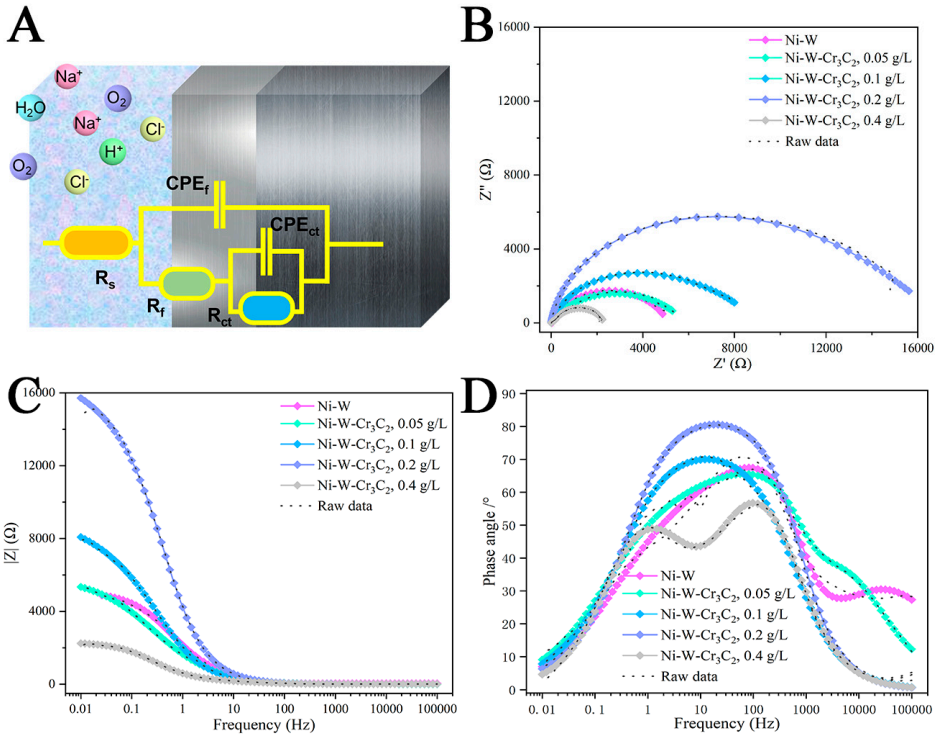


Figure 12. The EIS test in the brine containing 3.5% NaCl of the Ni-W-Cr_3C_2 electrodeposits with different concentrations of Cr_3C_2 particles in the bath: (**A**) equivalent circuit model, (**B**) Nyquist plot, (**C**) Bode plot, and (**D**) Bode-angle plot.

The arcs observed in the high-mid-frequency region of the Nyquist plot reflect the charge transfer impedance of the electrode with respect to the Faraday reaction (Figure 12). The ohmic impedance of this electrode and solution at the test polarization potential can be estimated from the intersection of the spectral line in the high-frequency region with the real axis. As for the bode plot, it is generally accepted that the impedance value in the low-frequency region (i.e., 0.01 Hz) reflects the corrosion resistance of the coating. Generally, the larger the impedance value is, the better the corrosion resistance is. For the majority of Ni-W composite coatings strengthened by the application of chromium carbide, it can be observed that the impedance values are greater than those of the pure alloy deposits, and the best corrosion resistance of the constructed composite coatings is obtained at a Cr_3C_2 concentration of 0.2 g/L. This result confirms that the introduction of diffuse phase particles of chromium carbide can improve the corrosion resistance of the coatings due to the increase in the thickness of the coatings, the effect of diffuse reinforcement, and the formation of corrosion-resistant oxide film layers. The introduction of dispersed phase particles has the potential to enhance the surface integrity and structural densification of deposited films [25,27]. Furthermore, the literature indicates that dispersed phase reinforcement enhances the strength of deposited films [28], which, in turn, improves the corrosion resistance of the deposited films. However, when the concentration of Cr_3C_2 in the plating solution increases to 0.4 g/L, the impedance value of the obtained Ni-W-Cr_3C_2 coating decreases significantly. This may be attributed to the fact that excessive hard particle clusters tend to be detached from the surface of the deposits during the deposition process, which increases the number of pores on the surface of the deposits and results in the degradation of the properties of the deposited coatings.

When the 3.5% NaCl solution is subjected to the constant injection of CO_2, the resulting saturation of the aqueous phase with CO_2 results in the dissolution of CO_2 into the aqueous phase, thereby generating carbonic acid. This process ultimately leads to the corrosion of carbon steel columns. The pH of a CO_2-saturated aqueous solution is

approximately 3.5~4.5 at room temperature at 25 °C, and the corrosion process is illustrated in Equations (1) and (7)–(11):

$$CO_2 + H_2O \rightarrow H_2CO_3 \quad (7)$$

$$H_2CO_3 \rightarrow H^+ + HCO_3^- \quad (8)$$

$$HCO_3^- \rightarrow CO_3^{2-} + H^+ \quad (9)$$

$$2H^+ + 2e^- \rightarrow H_2 \quad (10)$$

$$Fe^{2+} + CO_3^{2-} \rightarrow FeCO_3 \quad (11)$$

When nickel-deposited films are exposed to carbon dioxide, the dissolution of nickel results in the rapid depletion of H^+ on the film surface. This leads to an increase in surface pH, corresponding to an increase in the surface OH^- concentration. In this instance, an alkaline environment may develop on the films' surface, which facilitates nickel hydration and the formation of stable $Ni(OH)_2$. Thus, $Ni(OH)_2$/NiO layers can be formed by the recognized hydroxyl ligand mechanism [40–43]:

$$Ni + H_2O \rightarrow (NiOH)_{ads} + H^+ + e^- \quad (12)$$

$$(NiOH)_{ads} \rightarrow (NiOH)_{ads}^+ + e^- \quad (13)$$

$$(NiOH)_{ads}^+ + H_2O \rightarrow Ni(OH)_2 + H^+ \quad (14)$$

$$Ni(OH)_2 \rightarrow NiO + H_2O \quad (15)$$

The literature reveals that the main components of the passive film on nickel and nickel-based alloys in acidic environments are $Ni(OH)_2$ and NiO. Passive film can significantly impede the transfer rate of cations from the oxide matrix to the aqueous phase, thereby safeguarding the metal. This is because any dissolution must occur via the passive film in accordance with the dissolution kinetics of the passivating oxide [40]. The CO_2 corrosion effect is significantly mitigated despite the dissolution of CO_2, providing the essential H+ for the hydrogen evolution reactions and the cathodic reactions for the corrosion process. However, the relatively high content of $Ni(OH)_2$ in the $Ni(OH)_2$/NiO layer is likely to have a detrimental effect on the film's protective properties. This is because $Ni(OH)_2$ is less protective than NiO and allows the access of aggressive ions to the deposited film's surface.

In the aforementioned circumstances, Ni-W-Cr_3C_2 coatings are also subjected to a more severe corrosion risk. Indeed, a significant decrease in the film resistance values of all deposited coatings can be observed in the EIS test curves of the CO_2-saturated 3.5% NaCl solution, as displayed in Figure 13 and Table 3 because the formation of multiple types of oxide film layers (such as NiO, $Ni(OH)_2$, WO_3 and Cr_2O_3) may fail due to the acidic environment (Figure 14). In solutions saturated with CO_2, the oxygen content is extremely low, and these oxide films are difficult to repair rapidly. In corrosive media, this ultimately results in the dissolution of the deposit film. However, in the extremely harsh carbon dioxide corrosion environment, when the concentration of Cr_3C_2 in the electrolytic bath is set to 0.1 g/L or 0.2 g/L, the impedance value of the prepared Ni-W-Cr_3C_2 electrodeposits show a significant increase of about 45% compared with that of the pure alloy electrodeposits. This result indicates that Ni-W-Cr_3C_2 coatings have excellent corrosion resistance performance, which highlights its potential application as a corrosion-resistant material.

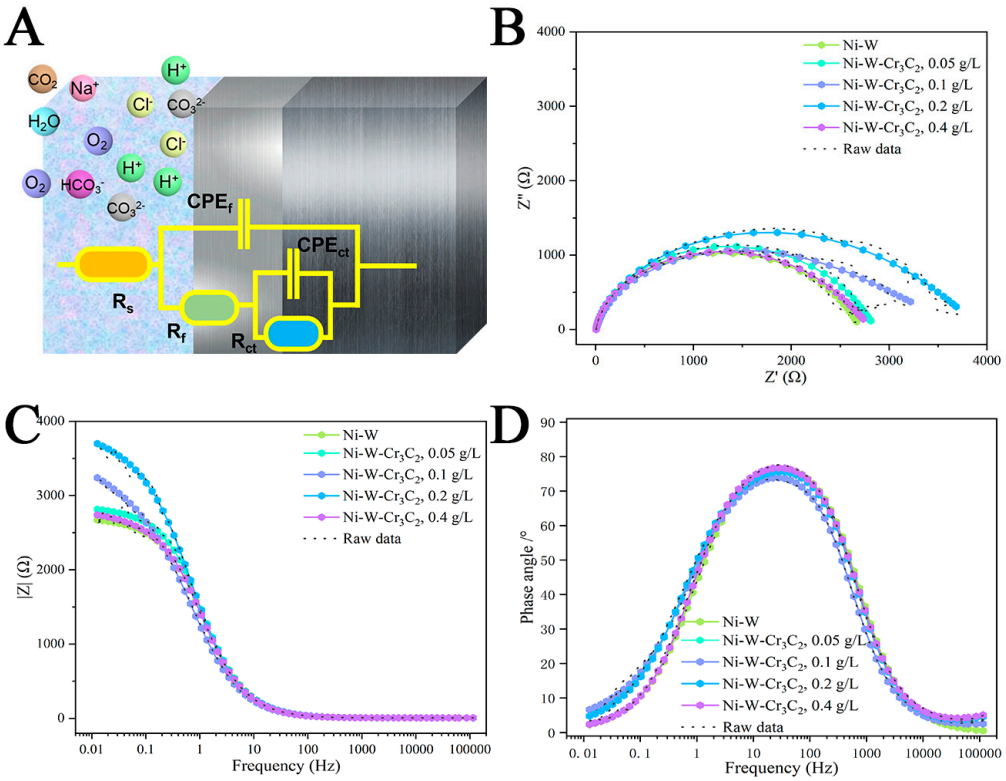


Figure 13. The EIS test in CO_2-saturated brine contain 3.5% NaCl of the Ni-W-Cr_3C_2 electrodeposits with different concentrations of Cr_3C_2 particles in the bath: (**A**) equivalent circuit model, (**B**) Nyquist plot, (**C**) Bode plot, and (**D**) Bode-angle plot.

Table 3. The equivalent circuit model parameters of the EIS test in the CO_2-saturated brine contain 3.5% NaCl of the Ni-W-Cr_3C_2 coatings.

Cr_3C_2 Amount	R_s (Ω)	CPE_f ($\Omega^{-1}\cdot cm^{-2}\cdot s^n$)	R_f (Ω)	CPE_{ct} ($\Omega^{-1}\cdot cm^{-2}\cdot s^n$)	R_{ct} (Ω)	R (Ω)
0	5.208	8.013×10^{-5}	3.624	3.661×10^{-4}	2713	2722
0.05	2.495	3.651×10^{-5}	5.47	0.983×10^{-4}	2883	2891
0.1	1.297	1.239×10^{-4}	6.499	9.054×10^{-5}	3841	3849
0.2	1.317	7.544×10^{-5}	4.548	7.196×10^{-5}	3983	3990
0.4	5.238	5.645×10^{-5}	5.882	7.416×10^{-4}	2855	2866

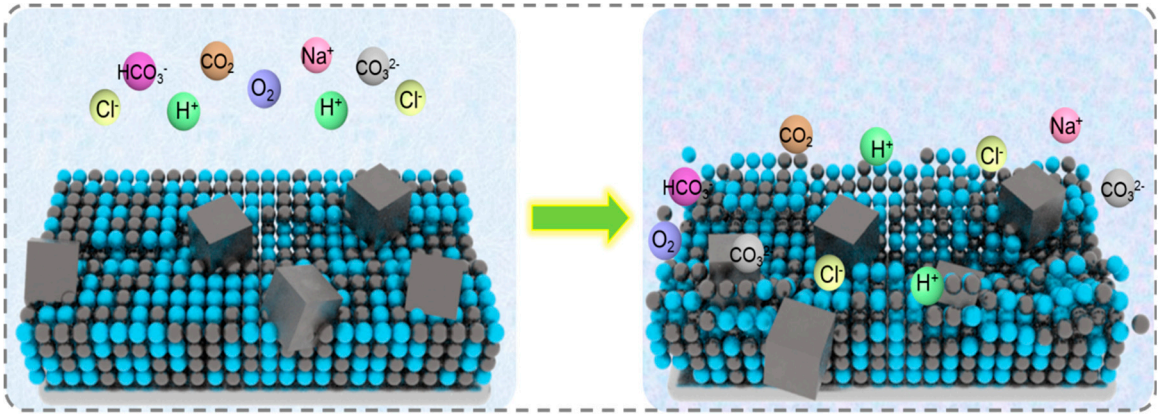


Figure 14. Schematic diagram of Ni-W-Cr_3C_2 electrodeposit failure process in saturated CO_2 brine.

4. Discussion

The utilization of hard particles of Cr_3C_2 for the diffuse phase reinforcement of Ni-W electrodeposits has been demonstrated to enhance the corrosion resistance of the coating. The newly designed electrodeposited coating exhibited a thickness that was approximately 30% greater than that of the original alloy coating. Additionally, the surface morphology and structural densities were optimized.

XRD analyses demonstrated that Cr_3C_2 particles were successfully embedded into the Ni-W deposit film. The primary components of the electrodeposits were identified as FCC nickel and BCC tungsten, which were dispersed as a solid solution in the nickel matrix. XPS analysis indicated the multiple types of dense oxide film layers (such as NiO, $Ni(OH)_2$, WO_3, and Cr_2O_3) that appeared in the surface of electrodeposits.

In order to evaluate the corrosion resistance of Ni-W-Cr_3C_2 electrodeposits, we employed EIS to ascertain their electrochemical anti-corrosion behavior, and the test medium consisted of two cases: the 3.5% NaCl solution and CO_2-saturated 3.5% NaCl solution. For the majority of Ni-W composite coatings strengthened by the application of chromium carbide, it can be observed that the impedance values are greater than those of the pure alloy deposits, and the best corrosion resistance of the constructed composite coatings is obtained at a Cr_3C_2 concentration of 0.2 g/L.

In this study, we also conducted a systematic comparison of the EIS properties of several types of Ni-W composite electrodeposits in conventional corrosive media [44–55], with a particular focus on the impedance value as a key parameter. As illustrated in Figure 15, the experimental outcomes demonstrate that the incorporation of chromium carbide as an additive significantly enhances the corrosion resistance of Ni-W deposits, as evidenced by elevated impedance values in comparison to carbon nanomaterials, nanosheet structure materials, and the majority of ceramic particle-reinforced systems. The observed phenomenon may be attributed to the distinctive advantages of Cr_3C_2 particles, including their particle size distribution, surface charge characteristics, and a series of extraordinary physicochemical properties, which act in concert to enable Cr_3C_2 to fulfill its role as a diffusely reinforcing phase, thereby effectively enhancing the corrosion resistance of Ni-W deposits, and thus providing a robust guarantee of the material's long-term service in a corrosive environment.

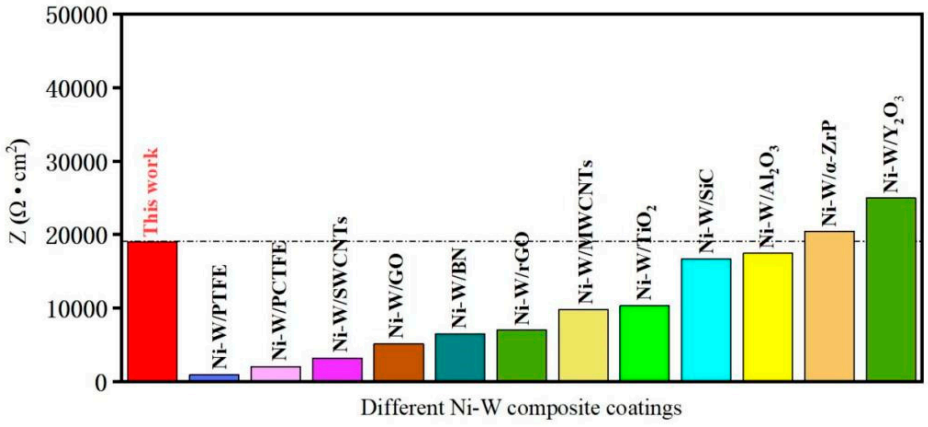


Figure 15. Comparison of impedance values of Ni-W-Cr_3C_2 electrodeposits and other composite electrodeposits.

5. Conclusions

1. Ni-W/Cr_3C_2 composite electrodeposits were prepared with corrosion resistance using the pulsed composite electrodeposition technique and the principle of diffuse phase strengthening. The results demonstrate that the Cr_3C_2 particles are capable of forming a sufficiently stable colloidal system in the bath. The impact of Cr_3C_2 as a dispersed phase on the micro-morphology, profile undulation, physical phase composition,

and surface chemical state of the Ni-W composite coatings is analyzed in detail. XPS analysis indicated the multiple types of dense oxide film layers (such as NiO, $Ni(OH)_2$, WO_3, and Cr_2O_3) that appeared on the surface of electrodeposits. The EIS results demonstrate that this dense oxide film can provide resistance to corrosive media containing chloride ions. However, in a humid environment saturated with carbon dioxide, the oxide film is highly susceptible to failure in acidic environments, which consequently reduces the corrosion resistance of the deposited coatings. Our findings revealed that the formation of a dense oxide film layer on the surface of electrodeposited materials is a key factor in maintaining their excellent corrosion resistance properties.

2. It is important to note that although Cr_3C_2 exhibits a significant strengthening effect on Ni-W electrodeposits, it is crucial to control its concentration during the deposition process. It was observed that when the concentration of Cr_3C_2 particles is excessively high, they are prone to agglomeration, which results in increased de-attachment during the deposition process. This phenomenon introduces defects, such as voids on the surface of the electrodeposited layer, which consequently affects the overall performance. Consequently, it was determined that the optimal addition amount of Cr_3C_2 particles in the electrolyte was 0.2 g/L. The Ni-W/Cr_3C_2 composite electrodeposits prepared under these conditions exhibited optimal electrochemical corrosion resistance, which provides an important reference for the design and application of these materials in related fields.

Author Contributions: Conceptualization, H.L. and W.Z.; methodology, X.Y.; software, P.L.; validation, W.H. and H.H.; formal analysis, H.L.; investigation, H.H.; resources, H.L.; data curation, W.Z.; writing—original draft preparation, H.L.; writing—review and editing, W.Z.; visualization, H.H.; supervision, X.Y.; project administration, H.L.; funding acquisition, H.L. All authors have read and agreed to the published version of the manuscript.

Funding: This work was supported by the Science and Technology Plan Project of Southwest Oil & Gasfield Company (2024D112-01-03).

Institutional Review Board Statement: Not applicable.

Informed Consent Statement: Not applicable.

Data Availability Statement: Data is contained within the article.

Acknowledgments: We were assisted by Yi He -from Southwest University of Petroleum (SWUP).

Conflicts of Interest: Hongjie Li, Xi Yuan, Puzhi Li, Weilei Han and Hongbing Huang are employed PetroChina Southwest Oil & Gasfield. Weizhi Zhang is employed by PetroChina Oil, Gas & New Energies Company. The authors declare that this study received funding from Science and Technology Plan Project of Southwest Oil & Gasfield Company. The funder was not involved in the study design, collection, analysis, interpretation of data, the writing of this article or the decision to submit it for publication.

References

1. Jones, M.W.; Peters, G.P.; Gasser, T.; Andrew, R.M.; Schwingshackl, C.; Gütschow, J.; Houghton, R.A.; Friedlingstein, P.; Pongratz, J.; Le Quéré, C. National contributions to climate change due to historical emissions of carbon dioxide, methane, and nitrous oxide since 1850. *Sci. Data* **2023**, *10*, 155. [CrossRef] [PubMed]
2. Barriopedro, D.; García-Herrera, R.; Ordóñez, C.; Miralles, D.G.; Salcedo-Sanz, S. Heat waves: Physical understanding and scientific challenges. *Rev. Geophys.* **2023**, *61*, e2022RG000780. [CrossRef]
3. Liu, Z.; Deng, Z.; Davis, S.; Ciais, P. Monitoring global carbon emissions in 2022. *Nat. Rev. Earth Environ.* **2023**, *4*, 205–206. [CrossRef] [PubMed]
4. Armstrong McKay, D.I.; Staal, A.; Abrams, J.F.; Winkelmann, R.; Sakschewski, B.; Loriani, S.; Cornell, S.E.; Rockstrom, J.; Lenton, T.M. Exceeding 1.5 °C global warming could trigger multiple climate tipping points. *Science* **2022**, *377*, eabn7950. [CrossRef] [PubMed]
5. Meinshausen, M.; Lewis, J.; McGlade, C.; Gütschow, J.; Nicholls, Z.; Burdon, R.; Cozzi, L.; Hackmann, B. Realization of Paris Agreement pledges may limit warming just below 2 °C. *Nature* **2022**, *604*, 304–309. [CrossRef]

6. Song, D.; Jiang, T.; Rao, C. Review of policy framework for the development of carbon capture, utilization and storage in China. *Int. J. Environ. Res. Public Health* **2022**, *19*, 16853. [CrossRef]
7. Jiang, K.; Ashworth, P.; Zhang, S.; Liang, X.; Sun, Y.; Angus, D. China's carbon capture, utilization and storage (CCUS) policy: A critical review. *Renew. Sustain. Energy Rev.* **2020**, *119*, 109601. [CrossRef]
8. Wang, P.; Shi, B.; Li, N.; Kang, R.; Li, Y.; Wang, G.; Yang, L. CCUS development in China and forecast its contribution to emission reduction. *Sci. Rep.* **2023**, *13*, 17811. [CrossRef]
9. Deng, Q.; Ling, X.; Zhang, K.; Tan, L.; Qi, G.; Zhang, J. CCS and CCUS technologies: Giving the oil and gas industry a green future. *Front. Energy Res.* **2022**, *10*, 919330. [CrossRef]
10. Adu, E.; Zhang, Y.; Liu, D. Current situation of carbon dioxide capture, storage, and enhanced oil recovery in the oil and gas industry. *Can. J. Chem. Eng.* **2019**, *97*, 1048–1076. [CrossRef]
11. Yan, T.; Xu, L.C.; Zeng, Z.X.; Pan, W.G. Mechanism and anti-corrosion measures of carbon dioxide corrosion in CCUS: A review. *iScience* **2024**, *27*, 108594. [CrossRef] [PubMed]
12. Xhanari, K.; Wang, Y.; Yang, Z.; Finšgar, M. A review of recent advances in the inhibition of sweet corrosion. *Chem. Rec.* **2021**, *21*, 1845–1875. [CrossRef] [PubMed]
13. Wang, W.; Guang, Y.; Liu, W.; Shen, K.; Huffman, M.; Wang, Q. Experimental investigation of stress corrosion on supercritical CO_2 transportation pipelines against leakage for CCUS applications. *Energy Rep.* **2023**, *9*, 266–276. [CrossRef]
14. Zhou, Y.; Xie, F.; Wang, D.; Wang, Y.; Wu, M. Carbon capture, utilization and storage (CCUS) pipeline steel corrosion failure analysis: A review. *Eng. Fail. Anal.* **2023**, *155*, 107745. [CrossRef]
15. Craig, B.; Rowe, A.; Warmack, M.; Doll, T.E.; Stevens, C.; Connors, K.C. Guidelines for the selection of corrosion resistant alloys for CCS and CCUS injection wells. *Int. J. Greenh. Gas Control.* **2023**, *129*, 103988. [CrossRef]
16. Wang, H.; Zhang, L.; Mei, K.; Cheng, X.; Xue, Q.; Wang, Y.; Fu, X. Recent progress on the research of steel corrosion behavior and corrosion control in the context of CO_2 geological utilization and storage: A review. *Corros. Rev.* **2024**, *42*, 435–454. [CrossRef]
17. Usman, B.J.; Ali, S.A. Carbon dioxide corrosion inhibitors: A review. *Arab. J. Sci. Eng.* **2018**, *43*, 1–22. [CrossRef]
18. Kang, Y.; Leng, X.; Zhao, L.; Bai, B.; Wang, X.; Chen, H. Review on the corrosion behaviour of nickel-based alloys in supercritical carbon dioxide under high temperature and pressure. *Crystals* **2023**, *13*, 725. [CrossRef]
19. Cui, G.; Yang, Z.; Liu, J.; Li, Z. A comprehensive review of metal corrosion in a supercritical CO_2 environment. *Int. J. Greenh. Gas Control.* **2019**, *90*, 102814. [CrossRef]
20. Tang, S.; Zhu, C.; Cui, G.; Xing, X.; Mu, J.; Li, Z. Analysis of internal corrosion of supercritical CO_2 pipeline. *Corros. Rev.* **2021**, *39*, 219–241. [CrossRef]
21. Li, W.; Luo, W.; Wang, D.; Wang, C.; Liu, Y.; Wen, L. Corrosion behavior of Ni-W coatings with and without macroscopic defects under different corrosion conditions. *Int. J. Electrochem. Sci.* **2024**, *19*, 100613. [CrossRef]
22. Fu, A.Q.; Feng, Y.R.; Cai, R.; Yuan, J.T.; Yin, C.X.; Yang, D.M.; Long, Y.; Bai, Z.Q. Downhole corrosion behavior of Ni-W coated carbon steel in spent acid & formation water and its application in full-scale tubing. *Eng. Fail. Anal.* **2016**, *66*, 566–576.
23. Liu, R.; Wang, H.; Li, X.P.; Ding, G.F. Study of internal stress of amorphous Ni–W alloy films. *Mater. Sci. Technol.* **2009**, *25*, 960–968. [CrossRef]
24. Li, H.; He, Y.; Luo, P.; Fan, Y.; Yu, H.; Wang, Y.; He, T.; Li, Z.; Zhang, H. Influence of pulse frequency on corrosion resistance and mechanical properties of Ni-W/B4C composite coatings. *Colloids Surf. A Physicochem. Eng. Asp.* **2021**, *629*, 127436. [CrossRef]
25. Cheng, X.; He, Y.; Song, R.; Li, H.; Liu, B.; Zhou, H.; Yan, L. Study of mechanical character and corrosion properties of La_2O_3 nanoparticle reinforced Ni-W composite coatings. *Colloids Surf. A Physicochem. Eng. Asp.* **2022**, *652*, 129799. [CrossRef]
26. Gong, X.; He, Y.; Yan, L.; Li, H.; Cheng, X.; He, Y.; Gou, R.; Yan, W. Study on mechanical properties and corrosion resistance of VC nanoparticles reinforced Ni-W coatings. *J. Solid State Electrochem.* **2023**, *27*, 3569–3582. [CrossRef]
27. Li, H.; Wen, S.; Yu, Z.; Hu, J.; Yan, J.; Ren, X. Preparation of $MoSi_2$-particle reinforced Ni-W alloy coatings and their anti-corrosion behavior in CO_2-saturated 3.5% NaCl solution. *Int. J. Electrochem. Sci.* **2024**, *19*, 100708. [CrossRef]
28. Xu, S.; Li, H.; He, Y.; Yan, S.; Cheng, X.; Chen, W.; Yan, J.; Wu, G.; Yuan, X. Exploring the mechanisms and characteristics of enhanced anti-corrosion and abrasion resistance of Ni-W coatings reinforced with Mg-Al LDH. *Vacuum* **2024**, *222*, 113031. [CrossRef]
29. Raihanuzzaman, R.M.; Xie, Z.; Hong, S.J.; Ghomashchi, R. Powder refinement, consolidation and mechanical properties of cemented carbides-An overview. *Powder Technol.* **2014**, *261*, 1–13. [CrossRef]
30. Zhang, L.; Gao, K.; Elias, A.; Dong, Z.; Chen, W. Porosity dependence of elastic modulus of porous Cr_3C_2 ceramics. *Ceram. Int.* **2014**, *40*, 191–198. [CrossRef]
31. Hirota, K.; Mitani, K.; Yoshinaka, M.; Yamaguchi, O. Simultaneous synthesis and consolidation of chromium carbides (Cr_3C_2, Cr_7C_3 and $Cr_{23}C_6$) by pulsed electric-current pressure sintering. *Mater. Sci. Eng. A* **2005**, *399*, 154–160. [CrossRef]
32. Hong, S.Y.; Nahm, S.; Oh, Y.S. Effect of heat treatment on the wear behavior of WC-Ni-Cr and WC-Ni-Cr + Cr_3C_2 coatings fabricated by high-velocity oxy-fuel method. *J. Korean Ceram. Soc.* **2022**, *59*, 465–472. [CrossRef]
33. Ghosh, D.; Mitra, S.K. Plasma sprayed Cr_3C_2-Ni-Cr coating for oxidation protection of 2.25Cr-1Mo steel. *Surf. Eng.* **2015**, *31*, 342–348. [CrossRef]
34. Shoba, M.K.; Mohan, K.M.; Raj, P.P. Effect of Detonation-Sprayed Cr_3C_2 and Ni-Cr Coatings on Performance Properties of Gray Cast Iron Gears. *Met. Sci. Heat Treat.* **2022**, *64*, 51–55. [CrossRef]

35. Chong, K.; Zou, Y.; Wu, D.; Tang, Y.; Zhang, Y. Pulsed laser remelting supersonic plasma sprayed Cr_3C_2-NiCr coatings for regulating microstructure, hardness and corrosion properties. *Surf. Coat. Technol.* **2021**, *418*, 127258. [CrossRef]
36. Hosseinzadeh, M.; Jafari, A.; Esmailzadeh, M.; Mirzaei, A. Morphological and mechanical characterization of co-deposited Ni/Cr_3C_2-NiCr composite coatings. *Mater. Res. Express* **2019**, *6*, 086517. [CrossRef]
37. Hernández, V.A. An overview of surface forces and the DLVO theory. *ChemTexts* **2023**, *9*, 10. [CrossRef]
38. Xiao, N.; Guan, X.; Wang, D.; Yan, H.; Cai, M.; Jia, N.; Zhang, Y.; Esling, C.; Zhao, X.; Zuo, L. Impact of W alloying on microstructure, mechanical property and corrosion resistance of face-centered cubic high entropy alloys: A review. *Int. J. Miner. Metall. Mater.* **2023**, *30*, 1667–1679. [CrossRef]
39. Liu, X.; Xiang, Z.; Niu, J.; Xia, K.; Yang, Y.; Yan, B.; Lu, W. The corrosion behaviors of amorphous, nanocrystalline and crystalline Ni-W alloys coating. *Int. J. Electrochem. Sci.* **2015**, *10*, 9042–9048. [CrossRef]
40. Marcus, P. *Corrosion Mechanisms in Theory and Practice*, 3rd ed.; CRC Press: Boca Raton, FL, USA, 2012.
41. Guzmán, R.S.S.; Vilche, J.R.; Arvia, A.J. The kinetics and mechanism of the nickel electrode—III. The potentiodynamic response of nickel electrodes in alkaline solutions in the potential region of $Ni(OH)_2$ formation. *Corros. Sci.* **1978**, *18*, 765–778. [CrossRef]
42. Real, S.G.; Vilche, J.R.; Arvia, A.J. The characteristics of the potentiodynamic potential/current profiles obtained with the Ni/0.5N H_2SO_4 interface. A contribution to the mechanism of the electrode process. *Corros. Sci.* **1980**, *20*, 563–586. [CrossRef]
43. Sun, C.; Zeng, H.; Luo, J.L. Unraveling the effects of CO_2 and H_2S on the corrosion behavior of electroless Ni-P coating in $CO_2/H_2S/Cl^-$ environments at high temperature and high pressure. *Corros. Sci.* **2019**, *148*, 317–330. [CrossRef]
44. Sangeetha, S.; Kalaignan, G.P.; Anthuvan, J.T. Pulse electrodeposition of self-lubricating Ni-W/PTFE nanocomposite coatings on mild steel surface. *Appl. Surf. Sci.* **2015**, *359*, 412–419. [CrossRef]
45. Hosseini, M.G.; Teymourinia, H.; Farzaneh, A.; Khameneh-asl, S. Evaluation of corrosion, mechanical and structural properties of new Ni-W-PCTFE nanocomposite coating. *Surf. Coat. Technol.* **2016**, *298*, 114–120. [CrossRef]
46. Mohammadpour, Z.; Zare, H.R. Structural effect of different carbon nanomaterials on the corrosion protection of Ni-W alloy coatings in saline media. *New J. Chem.* **2018**, *42*, 5425–5432. [CrossRef]
47. Sarangi, C.K.; Sahu, B.P.; Mishra, B.K.; Mitra, R. Pulse electrodeposition and characterization of graphene oxide particle-reinforced Ni-W alloy matrix nanocomposite coatings. *J. Appl. Electrochem.* **2020**, *50*, 265–279. [CrossRef]
48. Li, H.; He, Y.; He, T.; Qing, D.; Luo, F.; Fan, Y.; Chen, X. Ni-W/BN(h) electrodeposited nanocomposite coating with functionally graded microstructure. *J. Alloys Compd.* **2017**, *704*, 32–43. [CrossRef]
49. Wang, B.; Ma, Y.; Ran, C.; Liu, G.; Hou, Z. Preparation and properties of Ni-W-rGO composite coatings. *Int. J. Electrochem. Sci.* **2019**, *14*, 1884–1896. [CrossRef] [PubMed]
50. Fan, Y.; He, Y.; Luo, P.; Shi, T.; Li, H. Pulse current electrodeposition and characterization of Ni-W-MWCNTs nanocomposite coatings. *J. Electrochem. Soc.* **2015**, *162*, D270. [CrossRef]
51. Kumar, K.A.; Kalaignan, G.P.; Muralidharan, V.S. Direct and pulse current electrodeposition of Ni-W-TiO_2 nanocomposite coatings. *Ceram. Int.* **2013**, *39*, 2827–2834. [CrossRef]
52. Li, B.; Zhang, W.; Zhang, W.; Huan, Y. Preparation of Ni-W/SiC nanocomposite coatings by electrochemical deposition. *J. Alloys Compd.* **2017**, *702*, 38–50. [CrossRef]
53. Allahyarzadeh, M.H.; Aliofkhazraei, M.; Rouhaghdam, A.S.; Torabinejad, V. Electrodeposition of Ni–W–Al_2O_3 nanocomposite coating with functionally graded microstructure. *J. Alloys Compd.* **2016**, *666*, 217–226. [CrossRef]
54. Li, H.; He, Y.; Luo, P.; Fan, Y.; Gou, L.; Li, Z.; Zhao, Y.; Liu, B.; He, T.; Zhang, H. Preparation of laminar α-ZrP nanosheets enhanced Ni-W nanocomposite coating and investigation of its mechanical and anti-corrosion properties. *Surf. Coat. Technol.* **2021**, *423*, 127590. [CrossRef]
55. Xing, S.; Wang, L.; Jiang, C.; Liu, H.; Zhu, W.; Ji, V. Influence of Y_2O_3 nanoparticles on microstructures and properties of electrodeposited Ni-W-Y_2O_3 nanocrystalline coatings. *Vacuum* **2020**, *181*, 109665. [CrossRef]

Disclaimer/Publisher's Note: The statements, opinions and data contained in all publications are solely those of the individual author(s) and contributor(s) and not of MDPI and/or the editor(s). MDPI and/or the editor(s) disclaim responsibility for any injury to people or property resulting from any ideas, methods, instructions or products referred to in the content.